

Electronic correlations and topological states at the interface of twisted bilayer graphene and chromium oxychloride

Minsheng Li(李旻晟), Zehao Jia(贾泽浩), Xiangyu Cao(曹翔宇), Qiang Ma(马强), Chang Jiang(蒋昶), Yuda Zhang(张钰达), Linfeng Ai(艾临风), Pengliang Leng(冷鹏亮), and Faxian Xiu(修发贤)

Citation: Chin. Phys. B, 2026, 35 (**2**): 027202. DOI: 10.1088/1674-1056/ae2116
http://cpb.iphy.ac.cn; http://iopscience.iop.org/cpb

What follows is a list of articles you may be interested in

Valley-dependent transport in a mescoscopic twisted bilayer graphene device

Wen-Xuan Shi(史文萱), Han-Lin Liu(刘翰林), and Jun Wang(汪军)
Chin. Phys. B, 2024, 33 (**1**): 017205. DOI: 10.1088/1674-1056/acf9e4

Emergence of correlations in twisted monolayer-trilayer graphene heterostructures

Zhang Zhou(周璋), Kenji Watanabe, Takashi Taniguchi, Xiao Lin(林晓), Jinhai Mao(毛金海), and Hong-Jun Gao(高鸿钧)
Chin. Phys. B, 2023, 32 (**9**): 097203. DOI: 10.1088/1674-1056/ace3a8

Tunable correlation in twisted monolayer-trilayer graphene

Dongdong Ding(丁冬冬), Ruirui Niu(牛锐锐), Xiangyan Han(韩香岩), Zhuangzhuang Qu(曲壮壮), Zhiyu Wang(王知雨), Zhuoxian Li(李卓贤), Qianling Liu(刘倩伶), Chunrui Han(韩春蕊), and Jianming Lu(路建明)
Chin. Phys. B, 2023, 32 (**6**): 067204. DOI: 10.1088/1674-1056/acc8c3

Correlated states in alternating twisted bilayer-monolayer-monolayer graphene heterostructure

Ruirui Niu(牛锐锐), Xiangyan Han(韩香岩), Zhuangzhuang Qu(曲壮壮), Zhiyu Wang(王知雨), Zhuoxian Li(李卓贤), Qianling Liu(刘倩伶), Chunrui Han(韩春蕊), and Jianming Lu(路建明)
Chin. Phys. B, 2023, 32 (**1**): 017202. DOI: 10.1088/1674-1056/ac9de4

SPECIAL TOPIC — Moiré physics in two-dimensional materials

Electronic correlations and topological states at the interface of twisted bilayer graphene and chromium oxychloride

Minsheng Li(李旻晟)[1], Zehao Jia(贾泽浩)[1], Xiangyu Cao(曹翔宇)[1], Qiang Ma(马强)[1], Chang Jiang(蒋昶)[1], Yuda Zhang(张钰达)[1], Linfeng Ai(艾临风)[1], Pengliang Leng(冷鹏亮)[1], and Faxian Xiu(修发贤)[1,2,3,4,†]

[1] *State Key Laboratory of Surface Physics and Department of Physics, Fudan University, Shanghai* 200433, *China*
[2] *Shanghai Research Center for Quantum Sciences, Shanghai* 201315, *China*
[3] *Institute for Nanoelectronic Devices and Quantum Computing, Fudan University, Shanghai* 200433, *China*
[4] *Zhangjiang Fudan International Innovation Center, Fudan University, Shanghai* 201210, *China*

(Received 9 October 2025; revised manuscript received 14 November 2025; accepted manuscript online 19 November 2025)

When two layers of graphene are stacked with a twist angle of approximately 1.1°, strong interlayer coupling gives rise to a pair of flat bands in twisted bilayer graphene (TBG), resulting in pronounced electron–electron interactions. At half filling of the flat bands, TBG exhibits correlated insulating states. Here, we investigate the electrical transport properties of heterostructures composed of TBG and the antiferromagnetic insulator chromium oxychloride (CrOCl), and propose a strategy to modulate the correlated insulating states in TBG. During the transition from a conventional phase to a strong interfacial coupling phase, kink-like features are observed in the charge neutrality point (CNP), correlated insulating state, and band insulating state. Under a perpendicular magnetic field, the system exhibits broadened quantum Hall plateaus in the strong interfacial coupling regime. Electrons localized in the CrOCl layer screen the bottom gate, rendering the carrier density in TBG less sensitive to variations in the bottom gate voltage. These phenomena are well captured by a charge-transfer model between TBG and CrOCl. Our results provide insights into the control of electronic correlations and topological states in graphene moiré systems via interfacial charge coupling.

Keywords: twisted bilayer graphene, correlated insulating state, CrOCl, interfacial coupling, charge transfer

PACS: 72.80.Vp, 73.63.–b, 73.43.–f

DOI: 10.1088/1674-1056/ae2116 **CSTR:** 32038.14.CPB.ae2116

1. Introduction

When two graphene layers are twisted relative to each other at a magic angle close to 1.1°, strong interlayer interactions induce ultra-flat bands in the low-energy region.[1] The emergence of these flat bands in momentum space significantly suppresses the electron kinetic energy, allowing electron–electron Coulomb interactions to dominate. As a result, a variety of strongly correlated quantum phenomena emerge, including unconventional superconductivity,[2–4] Mott insulating states,[1,5] ferromagnetism,[6–9] and the quantum anomalous Hall effect.[10] At half filling of the flat bands, electrons become localized within the superlattice formed by the moiré pattern, giving rise to correlated insulating states. These electronic properties can be tuned *in situ* by varying the twist angle,[11,12] applying electric fields,[6,13] or applying strain,[14] making twisted bilayer graphene (TBG) an ideal platform for exploring strongly correlated quantum states. Beyond homobilayer TBG, similar gate-tunable correlated states and wavefunction localization transitions have also been observed in more complex twisted multilayer graphene systems, such as twisted monolayer–bilayer graphene[15] and alternating twisted multilayer heterostructures.[16]

Chromium oxychloride (CrOCl) is a two-dimensional intralayer antiferromagnetic insulator.[17–19] First-principles calculations predict an indirect band gap of 2.80 eV for CrOCl.[20] Van der Waals heterostructures composed of CrOCl and other materials exhibit strong interfacial coupling and pronounced hole-doping effects. For example, monolayer graphene/CrOCl heterostructures display a transition from fan-like to cascade-like Landau levels.[21] Raman spectroscopy measurements revealed blue shifts in both the G and 2D peaks, accompanied by a reduction in the intensity ratio of the 2D peak to the G peak, confirming hole doping in graphene.[22] Bernal bilayer graphene/CrOCl heterostructures exhibit an unconventional correlated insulating state with resistance exceeding 1 GΩ.[23] CrOCl imposes a superlattice Coulomb potential on graphene, generating topologically non-trivial subbands, while interlayer Coulomb coupling stabilizes the CrOCl interface band.[24] Moreover, a magnetically tunable charge transfer mechanism has been revealed through high-precision capacitance measurements, where maximum hysteresis occurs during the magnetic phase transition of CrOCl from an antiferromagnetic

[†]Corresponding author. E-mail: Faxian@fudan.edu.cn

© 2026 Chinese Physical Society and IOP Publishing Ltd. All rights, including for text and data mining, AI training, and similar technologies, are reserved.

to a ferrimagnetic-like state.[25] Coupling between antiferromagnetic insulators and graphene has been theoretically predicted to host high-temperature quantum anomalous Hall effect, as the antiferromagnetic insulator can provide both broken time-reversal symmetry and spin–orbit coupling.[26] To date, however, interfacial coupling between CrOCl and twisted graphene systems has not yet been reported. The modulation of CrOCl-induced Coulomb coupling on the strongly correlated insulating states in moiré superlattice systems therefore remains unexplored.

Owing to the weakly dispersive flat bands in TBG, TBG/CrOCl heterostructures represent a promising platform for investigating strongly correlated electron transport. In this work, we study the electrical transport properties of TBG/CrOCl van der Waals heterostructures. By employing a dual-gate structure, we effectively tune the interfacial coupling strength, enabling controlled switching between a conventional phase and a strong interfacial coupling phase. Pronounced changes in the position and strength of insulating states are observed across different coupling regimes. Under a perpendicular magnetic field, the system exhibits broadened quantum Hall plateaus in the strong interfacial coupling regime. Furthermore, we construct a charge transfer model to elucidate the underlying mechanism of strong interfacial coupling responsible for these observations. Our results provide a viable route for controlling correlated and topological quantum states in graphene moiré systems via interfacial charge coupling.

2. Experiment

The TBG/CrOCl heterostructures were fabricated using a dry transfer technique. A schematic illustration of the device structure is shown in Fig. 1(a). The TBG was fabricated by rotating the sample stage by 1.3°, accounting for a systematic discrepancy of 0.1°–0.2° between the nominal and measured twist angles in our setup. The TBG was encapsulated between hexagonal boron nitride (h-BN) and CrOCl (thickness ∼ 40–50 nm), and subsequently transferred onto a silicon dioxide/silicon (SiO_2/Si) substrate. Multi-terminal device structures were then defined using standard nanofabrication techniques. A Hall-bar-like geometry was patterned by reactive ion etching (RIE) for 3.5 min at a pressure of 60 mTorr, a radio-frequency (RF) power of 60 W, and a CHF_3/O_2 gas flow of 40/6 sccm. Subsequently, 5 nm/65 nm thick titanium/gold (Ti/Au) layers were deposited by magnetron sputtering to form the contact electrodes and top gate. The h-BN/TBG/CrOCl device adopts a dual-gate configuration, allowing independent control of carrier density and displacement field.[27,28] The top and bottom gate dielectrics are h-BN and SiO_2 (with CrOCl), respectively. An optical micrograph of the fabricated h-BN/TBG/CrOCl device is shown in Fig. 1(b). All electrical measurements were performed in a Dynacool system with a base temperature of 1.8 K.

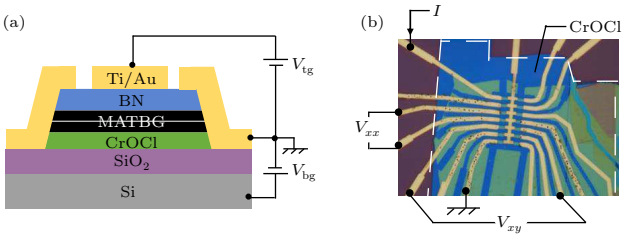


Fig. 1. (a) Schematic illustration of the h-BN/TBG/CrOCl device structure. (b) Optical micrograph of the fabricated device.

3. Results and discussion

3.1. Electrical transport properties of h-BN/TBG/CrOCl device under zero magnetic field conditions

We focus on the dual-gate phase diagram of the device at 0 T, shown in Fig. 2(a). The longitudinal resistance R_{xx} exhibits three bending peaks as the bottom gate voltage increases. According to the kink positions, we divide the dual-gate diagram into the conventional phase (left section) and the strong coupling phase (right section). In the conventional phase, the device exhibits typical TBG transport characteristics.[6] The three insulating regions — the charge neutrality point (CNP), the half-filling insulating state, and the superlattice insulating state — are almost unaffected by the displacement field $\boldsymbol{D}$ generated by the dual gates. Below the CNP region, hole conduction dominates, while above it electron conduction prevails. In this regime, there is almost no interlayer interaction between TBG and CrOCl, and CrOCl merely acts as a dielectric layer.

As the bottom gate voltage increases, the device transitions from the conventional phase to the strong coupling phase. The curved trajectories of the resistance peaks indicate that the relationship between gate voltage and charge carrier density in TBG is no longer linear or monotonic. Charge transfer occurs between TBG and CrOCl due to the interfacial coupling effect of CrOCl.[24] A significant number of electrons are transferred from TBG to the CrOCl surface, where they become localized by electron–electron interactions. In the right section of Fig. 2(a) ($V_{bg} \geq 0$ V), the V_{tg} corresponding to the CNP should be negative according to the trend observed in the conventional phase; however, the measured value becomes positive, indicating effective hole doping of the TBG. To clearly compare the evolution of resistance peaks between the conventional and strong coupling phases, we plot R_{xx} as a function of V_{tg} at fixed bottom gate voltages of −50 V (Fig. 2(b)) and 25 V (Fig. 2(c)). The resistance at the CNP increases from 22 kΩ to 217 kΩ, accompanied by a pronounced broadening of the corresponding gate voltage range. The resistance at the correlated insulator increases from 13 kΩ to 23 kΩ, whereas the resistance of

the superlattice insulating state increases only slightly, with its gate voltage range remaining almost unchanged. The significant enhancement of resistance at the CNP and the superlattice gap in the strong coupling phase can be attributed to two factors: enhanced electron–electron interactions induced by CrOCl through long-range Coulomb coupling, and the screening of charge impurities from the SiO_2 substrate by the CrOCl layer, which suppresses disorder scattering. In contrast, the correlated insulating state at half-filling is primarily driven by intrinsic electron correlations and is therefore less sensitive to this extrinsic disorder-screening effect. The transport properties exhibit a pronounced electron–hole asymmetry. This asymmetry originates from the asymmetric band alignment and charge transfer between TBG and CrOCl, and is further modulated by the gate-tunable interfacial coupling.

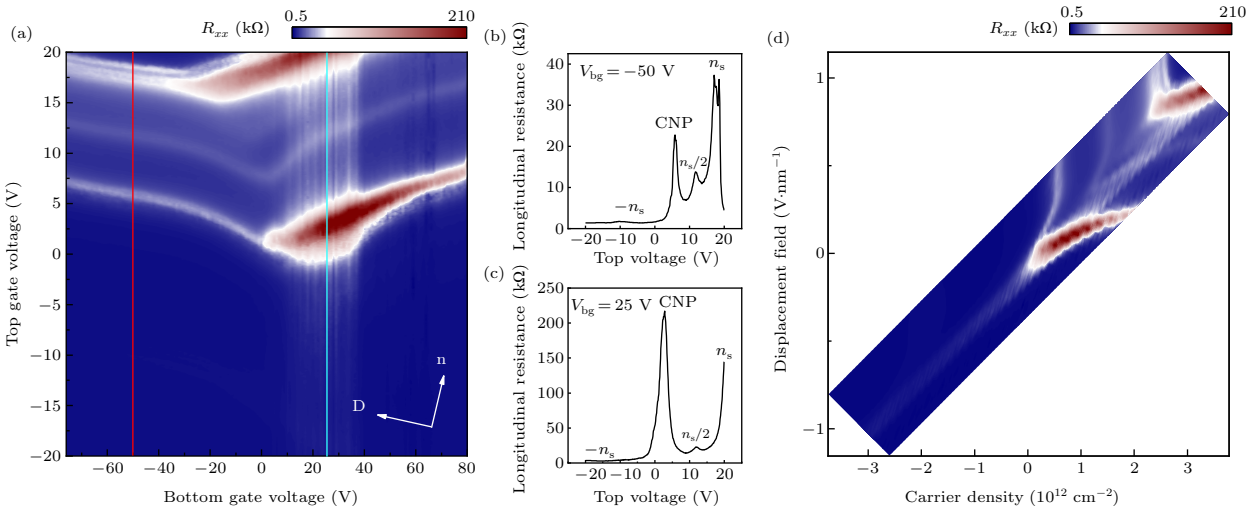


Fig. 2. (a) Dual-gate map of the longitudinal resistance R_{xx} measured at 2 K and 0 T. (b) R_{xx} as a function of the top gate voltage V_{tg} at a fixed bottom gate voltage of −50 V, corresponding to the red cutline in panel (a). (c) R_{xx} as a function of V_{tg} at a fixed bottom gate voltage of 25 V, corresponding to the blue cutline in panel (a). (d) $\boldsymbol{D}$–n phase diagram of R_{xx} as a function of the displacement field $\boldsymbol{D}$ and the carrier density n.

Based on the V_{tg} corresponding to the electron-side full-filling insulating state, the superlattice carrier density n_s required to fill each set of degenerate superlattice bands is deduced to be 2.66×10^{12} cm^{-2}. Each electronic band in the Brillouin zone of TBG possesses a four-fold degeneracy arising from spin and valley degrees of freedom.[29] Therefore, the superlattice carrier density is given by

$$n_s = 4/A \approx 8\theta^2/(\sqrt{3}a^2), \tag{1}$$

where the unit cell area A can be derived from graphene's hexagonal geometry, $A \approx \sqrt{3}a^2/\left(2\theta^2\right)$, a is the graphene lattice constant (0.246 nm), and θ is the twist angle.[2] From this relation, θ of the TBG is calculated to be 1.07°, which is close to the theoretical magic angle. It is worth noting that this calculation is performed in the conventional phase, where the CrOCl interface band lies above the Fermi level and no charge transfer occurs, ensuring that the deduced carrier density reflects solely the filling of the TBG moiré bands.

The dual-gate structure allows independent control of the carrier density and displacement field. The carrier density n and displacement field $\boldsymbol{D}$ are given by[28]

$$n = \left(C_{tg}V_{tg} + C_{bg}V_{bg}\right)/e, \tag{2}$$

$$\boldsymbol{D} = \left(C_{tg}V_{tg} - C_{bg}V_{bg}\right)/(2\varepsilon_0), \tag{3}$$

where C_{tg} and C_{bg} are the top and bottom gate capacitances per unit area, V_{tg} and V_{bg} are the voltages applied to the top and bottom gates, respectively, e is the electron charge, and ε_0 is the vacuum permittivity. From the slope of the resistance peaks in the conventional phase (Fig. 2(a), left section), we obtain the ratio of the bottom to top gate capacitances. We then transform the dual-gate diagram into a $\boldsymbol{D}$–n diagram. The relationship between R_{xx}, $\boldsymbol{D}$, and n is shown in Fig. 2(d). The displacement field can tune the interfacial coupling and charge transfer in the h-BN/TBG/CrOCl device. In the conventional phase, for the same n, the insulating states are almost independent of $\boldsymbol{D}$, indicating that $\boldsymbol{D}$ has a negligible effect on the band gap of TBG. In the strong coupling phase, R_{xx} is modulated by $\boldsymbol{D}$. The displacement field is screened by both free charges and the interlayer dielectric environment. When $\boldsymbol{D} = 0$, the h-BN/TBG/CrOCl heterostructure can be viewed as two monolayer graphenes without broken layer symmetry. As $\boldsymbol{D}$ increases, the heterostructure enters a layer-polarized state. At a critical $\boldsymbol{D}$, the interfacial band of CrOCl overlaps with the Fermi level of TBG, enabling charge transfer from TBG to the interfacial band. As a result, the doping capability of the dual gates on the electron side weakens.

4. Distinct quantum Hall behaviors in the conventional phase and strong-coupling phase under a perpendicular magnetic field

Under a perpendicular magnetic field, the motion of electrons is quantized in the plane perpendicular to the field, forming Landau levels. When the Fermi level lies within the gap between Landau levels, the longitudinal magnetoresistance approaches zero, and the Hall resistance exhibits quantized plateaus. The integer Hall plateau is given by

$$\nu = n_{\mathrm{TBG}} h/(eB), \tag{4}$$

where n_{TBG} is the TBG carrier concentration, h is Planck's constant, e is the elementary charge, and $\boldsymbol{B}$ is the magnetic field. We measure dual-gate maps of R_{xx} and R_{xy} at 5 T, as shown in Figs. 3(a) and 3(b). The quantum Hall behaviors in the two phases are distinct. In the conventional phase ($V_{\mathrm{bg}} \leq 0$), electrons in the h-BN/TBG/CrOCl device cannot move freely along the z-direction, and a series of integer quantum Hall effects (QHEs) under hole doping are observed. In the interfacial coupling phase ($V_{\mathrm{bg}} \geq 0$), a positive V_{bg} leads to a larger hole doping concentration in TBG. The rearrangement of interacting electrons in CrOCl may be the physical origin of this phenomenon.[24]

In the h-BN/TBG/CrOCl heterostructure, the integer Hall plateaus occur at $\nu = -4, -8, -12, \ldots$, as shown in Fig. 3(c). The negative integer filling factors indicate hole-type Hall transport, implying that CrOCl hole-dopes TBG. The spin and valley degeneracy is 4, consistent with the conventional Landau quantization behavior of TBG.

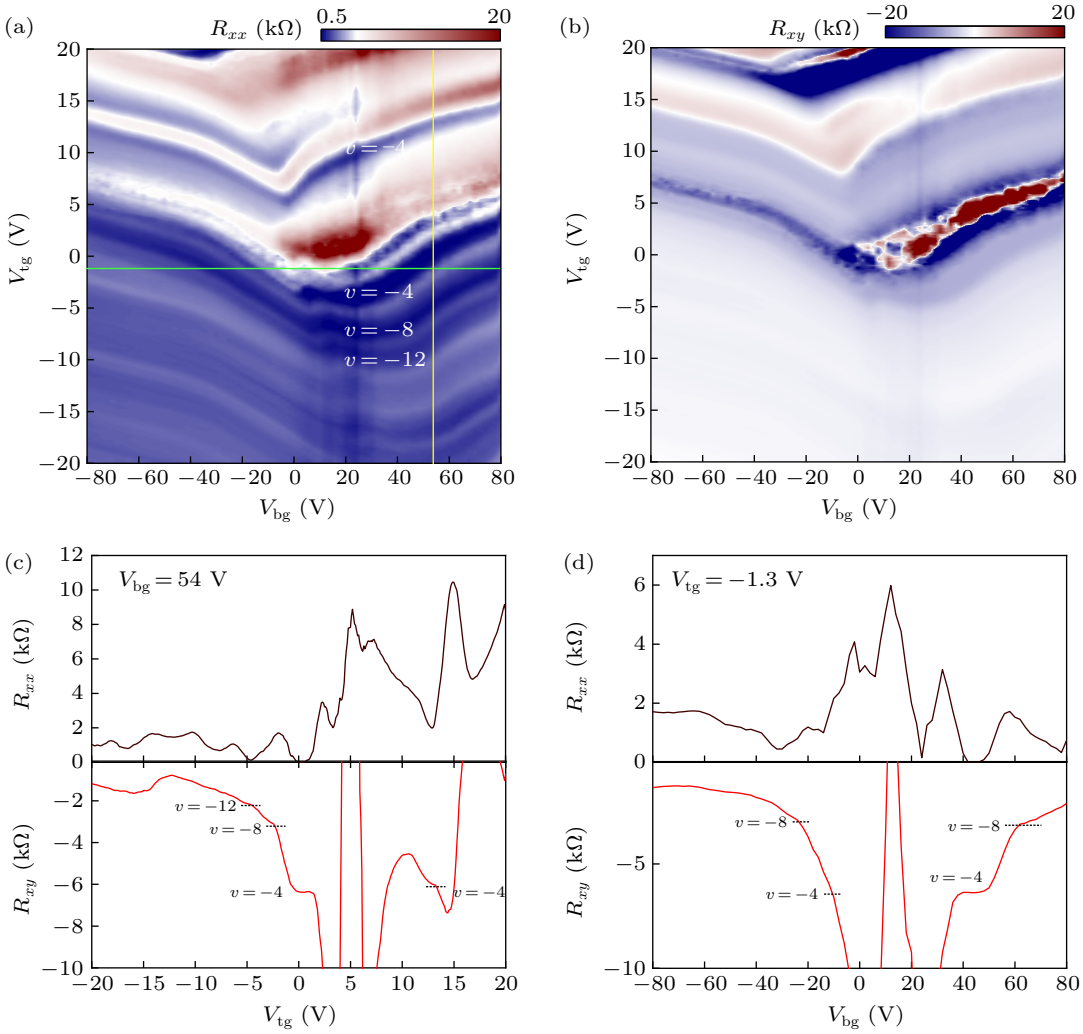


Fig. 3. (a) Dual-gate scan of R_{xx} at 2 K and 5 T. (b) Dual-gate scan of R_{xy} at 2 K and 5 T. (c) R_{xx} (upper panel) and R_{xy} (lower panel) as functions of V_{tg} at a fixed $V_{\mathrm{bg}} = 54$ V, corresponding to the yellow cutline in panel (a). (d) R_{xx} (upper panel) and R_{xy} (lower panel) as functions of V_{bg} at a fixed $V_{\mathrm{tg}} = -1.3$ V, corresponding to the green cutline in panel (a).

The conventional and strong coupling phases exhibit different quantum Hall effects, as shown in Fig. 3(d). Compared to the standard TBG quantum Hall plateaus, the plateaus at $\nu = -4$ and $\nu = -8$ in the strong coupling phase become wider. CrOCl can be considered an ideal dielectric layer at low temperatures. Electrons localized in CrOCl do not participate in transport, and charges applied by the gates do not accumulate in TBG but instead fill states within CrOCl.[30]

These electrons moving in the out-of-plane direction screen the back gate. For $\nu = -4$, the back gate cannot regulate the carrier concentration in TBG within the range from 38 V to 50 V, resulting in a widening of the quantum Hall plateau. This behavior further confirms that the nonlinear relationship between the dual-gate voltages and the carrier density in TBG originates from charge transfer into CrOCl, consistent with the trajectories of the insulating states observed in Fig. 2(a).

5. Charge transfer model between TBG and CrOCl

Based on the above experimental observations, we construct a charge transfer model between TBG and CrOCl to further understand the distinct behaviors of the device in the conventional and strong coupling phases. Figure 4(a) shows the phase diagram of interfacial coupling between TBG and CrOCl, compiled from the R_{xx} data measured under various V_{tg} and V_{bg} at 0 T. By tuning V_{tg} and V_{bg}, the system can reside in either the conventional phase I or the interfacial coupling phase II, indicated by blue and green regions in the phase diagram, respectively. In the conventional phase I region, the system exhibits typical dual-gate-dependent transport behavior of TBG. The CNP, half-filling correlated insulating state, and superlattice insulating state are observed and marked by white solid lines in the phase diagram. The black solid line denotes the phase boundary between the conventional and interfacial coupling phases, across which all insulating states exhibit bending. In the interfacial coupling phase II region, charge transfer between CrOCl and TBG occurs, making the TBG hole-doped and giving rise to unconventional gate-dependent transport properties. In region II, the resistance peaks at the CNP and superlattice insulating states increase significantly, accompanied by an expansion of their corresponding gate voltage ranges. Consequently, the CNP and superlattice insulating states evolve from conventional single-particle insulating states into quantum insulating states with enhanced electron–electron interactions.[23]

The work function difference between TBG and CrOCl determines their band alignment. Given that CrOCl possesses a high work function of 6.86 eV[31] and that Cl atoms are highly electronegative, CrOCl readily accepts electrons from TBG upon contact, resulting in carrier redistribution at the interface. As a strong electron acceptor, CrOCl effectively depletes electrons from TBG, shifting the Fermi level of TBG downward and thereby inducing hole doping. Figure 4(b) illustrates the electronic state occupation and band alignment of TBG and CrOCl under different combinations of dual-gate voltages. The blue shapes represent the flat and dispersive bands of TBG, with the Fermi level indicated by a black dashed line; states below the Fermi level are occupied by electrons. The green shapes represent the lowest-energy interface band of CrOCl, which does not contribute to electronic transport. Hybridization between the Cr 3d orbitals of CrOCl and the C 2p orbitals of TBG leads to the formation of interface states and consequent charge redistribution.[23] Applying a bottom-gate voltage is equivalent to establishing an electric field across the few-layer CrOCl, thereby shifting the CrOCl interface band relative to the Fermi level of TBG. When $V_{bg} < 0$ V, the negative gate voltage repels electrons in TBG toward the gate, raising the CrOCl interface band relative to the Fermi level. When $V_{bg} > 0$ V, the positive gate voltage attracts electrons in TBG toward the gate, lowering the CrOCl interface band relative to the Fermi level, and electrons gradually populate the interface band.

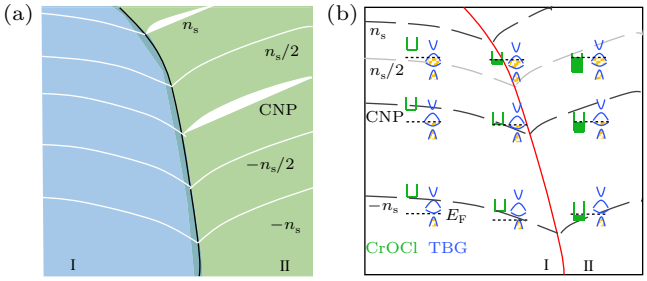


Fig. 4. (a) Dual-gate phase diagram of the h-BN/TBG/CrOCl device. Region I (blue) corresponds to the conventional phase, and Region II (green) corresponds to the interfacial coupling phase. The black solid line denotes the phase boundary between the two phases. The white solid lines mark the CNP, the half-filling correlated insulating state, and the superlattice insulating state. (b) Charge transfer model between TBG and CrOCl under dual-gate control, illustrating the band alignment of the interface states of TBG (blue) and CrOCl (green). The black dashed line indicates the Fermi level E_F of TBG, and the red solid line represents the phase boundary.

In the conventional phase I region, the CrOCl interface band lies above the Fermi level of TBG, and no charge transfer occurs between CrOCl and TBG. In this case, CrOCl acts only as a gate dielectric material. Its dielectric constant $\varepsilon \approx 4.9$[25] provides significant dielectric screening for TBG, reducing Coulomb scattering between electrons and charged impurities. Adjusting the dual-gate voltages enables capacitive doping of TBG in the usual manner, similar to that in standard h-BN/TBG/h-BN structures.[6]

In the interfacial coupling phase II region, the interface band of CrOCl introduces an additional capacitance. As the bottom gate voltage increases gradually, the CrOCl interface band begins to overlap with the Fermi level of TBG. Electrons transfer from TBG into CrOCl, and partial electronic states in CrOCl lie below the Fermi level of TBG. When $V_{tg} < 0$ V, the negative gate voltage repels electrons in TBG, lowering the Fermi level of TBG and increasing the hole doping concentration. As the absolute value of the negative gate voltage increases, the concentration of interfacial charge transfer gradually decreases. When $V_{tg} > 0$ V, the positive gate

voltage raises the Fermi level in TBG, and the concentration of electrons transferred from TBG to the CrOCl interface band increases correspondingly. As the gate voltage increases further, a correlated insulating state appears when the Fermi level of TBG reaches the half-filling position of the flat bands. A superlattice insulating state appears when each moiré unit cell is filled with four electrons. In the interfacial coupling phase, the interface band of CrOCl may form a long-wavelength localized charge order.[21] When filled with electrons, the interfacial band provides an effective background superlattice potential for electrons in TBG, enhancing the insulating states at the CNP and full-filling phase in the h-BN/TBG/CrOCl device.[24] Our findings in TBG/CrOCl heterostructures extend previous studies on CrOCl-based heterostructures. For instance, reconstructed Landau levels were observed in monolayer graphene/CrOCl,[21] while an unconventional correlated insulator was reported in Bernal bilayer graphene/CrOCl.[23] Interfacial charge coupling mechanisms across different graphene/CrOCl heterostructures are similar. In our twisted system, the interplay between the moiré flat bands and the CrOCl interfacial coupling leads to unique gate-tunable correlated and topological states, as well as modified quantum Hall behaviors in the strong coupling phase, highlighting the distinct physics arising from the twist angle.

6. Conclusion

In conclusion, the transition from a conventional phase to an interfacial coupling phase is demonstrated for TBG by varying the top and bottom gate voltages of h-BN/TBG/CrOCl van der Waals heterostructures. During the transition, bending phenomena are observed in the trajectories of the CNP, correlated insulating state, and band insulating state. CrOCl enhances electron–electron interactions in TBG through long-range interlayer Coulomb coupling, leading to an order-of-magnitude increase in resistance at the CNP and the superlattice insulating state in the interfacial coupling phase. Under a perpendicular magnetic field, the integer quantum Hall effect in TBG consistently shows negative filling factors, indicating hole doping of TBG due to charge transfer within the heterostructure. Broadened Landau level quantization plateaus are observed in the strong interfacial coupling phase, indicating that the quantum Hall effect is significantly influenced by the interaction between TBG and the underlying CrOCl. A charge transfer model between TBG and CrOCl is constructed to explain the transport phenomena. Charge redistribution at the interface stems from the work function mismatch between TBG and CrOCl. At the phase boundary between the conventional and interfacial coupling phases, the interfacial band of CrOCl overlaps with the Fermi level of TBG, enabling charge transfer from TBG to the CrOCl interface band. CrOCl acts as a source of holes for TBG. Electrons filling the interfacial bands in CrOCl form charge order, which promotes electron–electron interactions in TBG through long-range Coulomb coupling. This work provides experimental evidence for exploring the carrier control mechanism of correlated insulating states in twisted graphene and offers insights for future manipulation of electronic correlations and topological states in twisted graphene moiré systems through interfacial charge coupling.

Acknowledgments

Project supported by the National Natural Science Foundation of China (Grant Nos. 52225207 and 52350001), the Shanghai Pilot Program for Basic Research–Fudan University 21TQ1400100 (Grant No. 21TQ006), and the Shanghai Municipal Science and Technology Major Project (Grant No. 2019SHZDZX01).

References

[1] Cao Y, Fatemi V, Demir A, Fang S, Tomarken S L, Luo J Y, Sanchez-Yamagishi J D, Watanabe K, Taniguchi T, Kaxiras E, Ashoori R C and Jarillo-Herrero P 2018 *Nature* **556** 80
[2] Cao Y, Fatemi V, Fang S, Watanabe K, Taniguchi T, Kaxiras E and Jarillo-Herrero P 2018 *Nature* **556** 43
[3] Stepanov P, Das I, Lu X, Fahimniya A, Watanabe K, Taniguchi T, Koppens F H L, Lischner J, Levitov L and Efetov D K 2020 *Nature* **583** 375
[4] Saito Y, Ge J, Watanabe K, Taniguchi T and Young A F 2020 *Nat. Phys.* **16** 926
[5] Po H C, Zou L, Vishwanath A and Senthil T 2018 *Phys. Rev. X* **8** 31
[6] Sharpe A L, Fox E J, Barnard A W, Finney J, Watanabe K, Taniguchi T, Kastner M A and Goldhaber-Gordon D 2019 *Science* **365** 605
[7] Sharpe A L, Fox E J, Barnard A W, Finney J, Watanabe K, Taniguchi T, Kastner M A and Goldhaber-Gordon D 2021 *Nano Lett.* **21** 4299
[8] Tschirhart C L, Serlin M, Polshyn H, Shragai A, Xia Z, Zhu J, Zhang Y, Watanabe K, Taniguchi T, Huber M E and Young A F 2021 *Science* **372** 1323
[9] Grover S, Bocarsly M, Uri A, Stepanov P, Di Battista G, Roy I, Xiao J, Meltzer A Y, Myasoedov Y, Pareek K, Watanabe K, Taniguchi T, Yan B, Stern A, Berg E, Efetov D K and Zeldov E 2022 *Nat. Phys.* **18** 885
[10] Serlin M, Tschirhart C L, Polshyn H, Zhang Y, Zhu J, Watanabe K, Taniguchi T, Balents L and Young A F 2020 *Science* **367** 900
[11] Lu X, Stepanov P, Yang W, Xie M, Aamir M A, Das I, Urgell C, Watanabe K, Taniguchi T, Zhang G, Bachtold A, MacDonald A H and Efetov D K 2019 *Nature* **574** 653
[12] Pierce A T, Xie Y, Park J M, Khalaf E, Lee S H, Cao Y, Parker D E, Forrester P R, Chen S, Watanabe K, Taniguchi T, Vishwanath A, Jarillo-Herrero P and Yacoby A 2021 *Nat. Phys.* **17** 1210
[13] Rodan-Legrain D, Cao Y, Park J M, de la Barrera S C, Randeria M T, Watanabe K, Taniguchi T and Jarillo-Herrero P 2021 *Nat. Nanotechnol.* **16** 769
[14] Zhang Z, Wen L, Qiao Y and Li Z 2023 *Chin. Phys. B* **32** 107302
[15] Li S, Wang Z, Xue Y, Cao L, Watanabe K, Taniguchi T, Gao H and Mao J 2023 *Chin. Phys. B* **32** 067304
[16] Niu R, Han X, Qu Z, Wang Z, Li Z, Liu Q, Han C and Lu J 2023 *Chin. Phys. B* **32** 017202
[17] Zhang T, Wang Y, Li H, Zhong F, Shi J, Wu M, Sun Z, Shen W, Wei B, Hu W, Liu X, Huang L, Hu C, Wang Z, Jiang C, Yang S, Zhang Q M and Qu Z 2019 *ACS Nano* **13** 11353
[18] Gu P, Sun Y, Wang C, Peng Y, Zhu Y, Cheng X, Yuan K, Lyu C, Liu X, Tan Q, Zhang Q, Gu L, Wang Z, Wang H, Han Z, Watanabe K, Taniguchi T, Yang J, Zhang J, Ji W, Tan P H and Ye Y 2022 *Nano Lett.* **22** 1233
[19] Miao N, Xu B, Zhu L, Zhou J and Sun Z 2018 *J. Am. Chem. Soc.* **140** 2417

[20] Li S, Zhang J, Li Y, Zhang K, Zhu L, Gao W, Li J and Huo N 2023 *Appl. Phys. Lett.* **122** 083503
[21] Wang Y, Gao X, Yang K, Gu P, Lu X, Zhang S, Gao Y, Ren N, Dong B, Jiang Y, Watanabe K, Taniguchi T, Kang J, Lou W, Mao J, Liu J, Ye Y, Han Z, Chang K, Zhang J and Zhang Z 2022 *Nat. Nanotechnol.* **17** 1272
[22] Ying B, Xin B, Li M, Zhou S, Liu Q, Zhu Z, Qin S, Wang W H and Zhu M 2024 *ACS Appl. Mater. Interfaces* **16** 43806
[23] Yang K, Gao X, Wang Y, Zhang T, Gao Y, Lu X, Zhang S, Liu J, Gu P, Luo Z, Zheng R, Cao S, Wang H, Sun X, Watanabe K, Taniguchi T, Li X, Zhang J, Dai X, Chen J H, Ye Y and Han Z 2023 *Nat. Commun.* **14** 2136
[24] Lu X, Zhang S, Wang Y, Gao X, Yang K, Guo Z, Gao Y, Ye Y, Han Z and Liu J 2023 *Nat. Commun.* **14** 5550
[25] Cao S, Zheng R, Wang C, Ma N, Chen M, Song Y, Feng Y, Hao T, Zhang Y, Wang Y, Gu P, Watanabe K, Taniguchi T, Liu Y, Xie X C, Ji W, Ye Y, Han Z and Chen J H 2025 *Adv. Mater.* **37** e2411300
[26] Qiao Z, Ren W, Chen H, Bellaiche L, Zhang Z, Macdonald A H and Niu Q 2014 *Phys. Rev. Lett.* **112** 116404
[27] Maher P, Wang L, Gao Y, Forsythe C, Taniguchi T, Watanabe K, Abanin D, Papić Z, Cadden-Zimansky P, Hone J, Kim P and Dean C R 2014 *Science* **345** 61
[28] Zhang Y, Tang T T, Girit C, Hao Z, Martin M C, Zettl A, Crommie M F, Shen Y R and Wang F 2009 *Nature* **459** 820
[29] Bistritzer R and MacDonald A H 2011 *Proc. Natl Acad. Sci. USA* **108** 12233
[30] Tseng C C, Song T, Jiang Q, Lin Z, Wang C, Suh J, Watanabe K, Taniguchi T, McGuire M A, Xiao D, Chu J H, Cobden D H, Xu X and Yankowitz M 2022 *Nano Lett.* **22** 8495
[31] Liu D, Zhou Y, Zheng S, Liu X, Sun J, Li Z, Zhang Z, Zhang Z, Wang S, Cai D, Cheng Y and Huang W 2023 *ACS Appl. Electron. Mater.* **5** 3973